

A new candidate for central tidal disruption event in SDSS J014124+010306 with broad Mg II line at $z = 1.06$

Xue-Guang Zhang*

School of physical science and technology, GuangXi University, No. 100, Daxue Road, 530004, Nanning, P. R. China

11 August 2022

ABSTRACT

In the Letter, a new candidate for central tidal disruption event (TDE) is reported in SDSS J014124+010306 (=SDSS J0141) with broad Mg II line at redshift $z = 1.06$. Based on long-term photometric *ugriz*-band variabilities from SDSS Stripe82 Database and PHOTOOBJALL database, a central TDE is preferred with a $1.3M_{\odot}$ main-sequence star tidally disrupted by central black hole (BH) of $(14 \pm 2) \times 10^6 M_{\odot}$ in SDSS J0141. Moreover, CAR process has been applied to confirm that the probability is only about 0.4% that the long-term variabilities in SDSS J0141 are not related to TDE but from intrinsic AGN activities. Meanwhile, based on the apparent broad Mg II emission lines, virial BH mass can be estimated as $245 \times 10^6 M_{\odot}$, 18 times larger than the TDE-model determined BH mass, providing further clues to support a central TDE in SDSS J0141, similar as the case in the TDE candidate SDSS J0159 with virial BH mass two magnitudes larger than M-sigma relation expected BH mass. Among the reported optical TDE candidates, SDSS J0141 is the candidate at the highest redshift. The results in the Letter indicate it should be common to detect TDE candidates in high redshift galaxies with broad Mg II lines.

Key words: galaxies:nuclei - quasars:emission lines - transients: tidal disruption events - quasars: individual (SDSS J0141)

1 INTRODUCTION

TDEs (Tidal Disruption Events), indicators to massive black holes (BHs) and BH accreting systems, have been well studied in detail for more than four decades (Rees 1988; Loeb & Ulmer 1997; Gezari et al. 2006; Guillochon & Ramirez-Ruiz 2013; Guillochon et al. 2014; Mockler et al. 2019; Stone et al. 2019; Zhou et al. 2021) with accreting fallback debris from stars tidally disrupted by central black holes (BHs) leading to apparent time-dependent variabilities. More recent reviews on TDE can be found in Gezari (2021). More recent two large samples of dozens of new TDE candidates can be found in van Velzen et al. (2021) and in Sazonov et al. (2021).

Among the reported TDE candidates, almost all the candidates are reported in inactive galaxies, such as the two candidates in non-active galaxies through the Stripe82 database by van Velzen et al. (2011), the PS1-10jh and PS1-11af in inactive galaxies through the PanSTARRS (panoramic survey telescope and rapid response system) by Gezari et al. (2012); Chornock et al. (2014), the iPTF16fnl in E+A galaxy through the PTF (palomar transient factory) by Blagorodnova et al. (2017), the OGLE17aaj through the Optical Gravitational Lensing Experiment (OGLE) in quite weakly active galaxy by Gromadzki et al. (2019), and the well-known ASASSN-14ae, ASASSN-14li and ASASSN-19dj in nearby quiescent galaxies through the ASAS-SN (all-sky automated survey for supernovae) by Holoien et al. (2014, 2016); Hinkle et al. (2021), etc.. Besides the TDE candidates in quiescent galaxies, there are only a few TDE candidates reported in active galaxies, such as the SDSS J0159 (Merloni et al. 2015), CNSS J0019+00 (Anderson et al. 2020). However, in SDSS J0159, due to quite different virial BH mass from the M-sigma relation expected BH mass as discussed in Zhang et al.

(2019), the broad Balmer emission lines are expected to be totally related to central TDE debris, indicating SDSS J0159 is not a normal broad line AGN (BLAGN). And in CNSS J0019+00, there are no broad emission lines, indicating CNSS J0019+00 is not a normal broad line AGN. It is an interesting objective to detect TDE candidates in normal broad line galaxies.

Among the reported optical TDE candidates, strong broad Balmer and Helium emission lines are fundamental spectroscopic characteristics. And the reported broad emission lines can be related to disk-like structures from TDE debris, such as SDSS J0159 in Merloni et al. (2015); Zhang (2021), ASASSN-14li in Holoien et al. (2016), PTF09djl in Liu et al. (2017), PS18kh in Holoien et al. (2019), AT2018hyz in Short et al. (2020); Hung et al. (2020), etc., indicating the reported broad emission lines in the TDE candidates are not related to normal BLRs in normal BLAGN. Moreover, there are several TDE candidates, their UV-band spectra have been well checked, such as the PS18kh, ASASSN-15lh, ASASSN-14li, etc., there are no broad Mg II $\lambda 2800\text{\AA}$ emission lines. In other words, if there was broad Mg II emission line in UV spectra of a TDE candidate, the host galaxy of the TDE candidate could be probably a normal BLAGN. Therefore, to detect and report a TDE candidate with apparent broad Mg II line is the main objective of the Letter.

Among the high redshift objects in SDSS covering broad Mg II emissions, a new TDE candidate in J014124+010306 (=SDSS J0141) at a redshift of 1.06 is reported in the Letter. Section 2 presents the long-term photometric SDSS *ugriz*-band variabilities of SDSS J0141. Section 3 shows the theoretical TDE model and fitting procedure applied. Section 4 shows spectroscopic properties and necessary discussions. Section 5 gives our final conclusions. We have adopted the cosmological parameters of $H_0 = 70 \text{ km} \cdot \text{s}^{-1} \text{ Mpc}^{-1}$, $\Omega_{\Lambda} = 0.7$ and $\Omega_m = 0.3$.

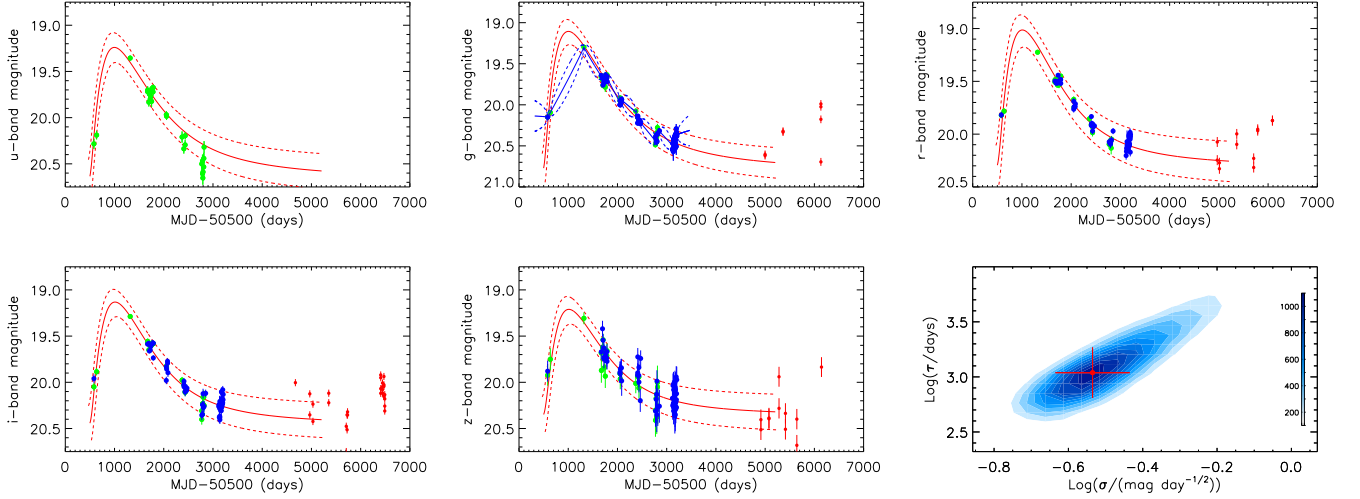


Figure 1. Top panels and bottom left two panels show the SDSS *ugriz*-band light curves and the TDE model determined best descriptions. In each panel, solid blue and green circles represent the data points from the Stripe82 database and from the PHOTOBJALL database, respectively. In each panel, solid and dashed red lines show the TDE model determined best descriptions and the corresponding confidence bands determined by uncertainties of the model parameters. In top middle panel, solid and dashed blue lines show the DRW process determined best descriptions to the *g*-band light curve and the corresponding 1sigma confidence bands. In each panel, solid circles plus error bars in red show the data points from the PanSTARRS, without considerations of magnitude difference between SDSS and PanSTARRS. Bottom right panel shows the two dimensional posterior distributions of the DRW process parameters of σ and τ with solid circle plus error bars in red marking the accepted values.

2 LONG-TERM LIGHT CURVES IN SDSS J0141

As a follow-up to our previous work on changing-look AGN in Zhang (2021b), plans are underway for systematic searching changing-look AGN through multi-epoch SDSS spectra. When checking long-term variabilities of the candidates, the SDSS J0141 with five repeated spectra is selected as the target of the Letter, due to its unique photometric variabilities.

SDSS *ugriz*-band light curves of SDSS J0141 are collected from the following two databases. First, the *griz*-band light curves are collected from the Stripe82 database (Bramich et al. 2008) with MJD from 51081 (September 1998) to 53705 (December 2005). There are no *u*-band data points provided by the Stripe82 database. Second, the *ugriz*-band variabilities are collected from the SDSS PHOTOBJALL database according to THINGID=120118318 and the corresponding 29 photometric objids of SDSS J0141, by the following query applied in the SQL search tool in SDSS DR16,

```
SELECT mjd, psfmag_g, psfmag_u, psfmag_r, psfmag_i, psfmag_z,
       psfmagerr_g, psfmagerr_u, psfmagerr_r, psfmagerr_i, psfmagerr_z
FROM PHOTOBJALL
WHERE objid = 1237657072231972919 or
       objid = 1237657192526905410 or objid = 1237657235444138067 or
       objid = 1237657364307247212 or objid = 1237657587628048446 or
       objid = 1237657737952297019 or objid = 1237657815264133192 or
       objid = 1237659915500454002 or objid = 1237660010022568005 or
       objid = 1237662969222070482 or objid = 1237663205462114377 or
       objid = 1237663506125488270 or objid = 1237663544780849275 or
       objid = 1237666302155292964 or objid = 1237666340803444954 or
       objid = 1237666383743484048 or objid = 1237666409527247014 or
       objid = 1237666499696328851 or objid = 1237666542643773631 or
       objid = 1237666637155991620 or objid = 1237666662926516356 or
       objid = 1237666727323500667 or objid = 1237646012704882989 or
       objid = 1237646648350802019 or objid = 1237653000602648648 or
       objid = 1237656513891467420 or objid = 1237656595492765803 or
       objid = 1237656909050544257 or objid = 1237656973454934076
```

Here, due to the point-like photometric images of SDSS J0141 at redshift 1.06, PSF magnitudes are collected from the PHOTOOB-

JALL, rather than the Petrosian magnitudes commonly accepted for extended photometric images.

The light curves are shown in Fig. 1. The rise-to-peak and followed by smooth declining trend in each band light curve is apparent and can be well expected by a central TDE. Then, the theoretical TDE model can be considered to describe the variabilities of SDSS J0141.

3 THEORETICAL TDE MODEL APPLIED TO DESCRIBE THE LIGHT CURVES

More recent detailed descriptions on theoretical TDE model can be found in Guillochon & Ramirez-Ruiz (2013); Guillochon et al. (2014); Mockler et al. (2019) and in the corresponding public codes of TDEFIT and the MOSFIT. Here, based on the more recent discussions in Mockler et al. (2019), the theoretical TDE model can be applied by the following four steps, similar what we have done in Zhang (2022) to describe the X-ray variabilities in the TDE candidate *Swift* J2058.4+0516 with relativistic jet.

First, standard templates of viscous-delayed accretion rates \dot{M}_{at} are created, based on the TDEFIT/MOSFIT provided the dm/de as distributions of debris mass dm as a function of the specific binding energy e after a star is disrupted, by the equations

$$\dot{M}_{at} = \frac{\exp(-t/T_v)}{T_v} \int_0^t \exp(t'/T_v) \dot{M}_{fbt} dt' \quad (1)$$

$$\dot{M}_{fbt} = dm/de \times de/dt \quad de/dt = \frac{(2\pi G M_{BH})^{2/3}}{3 t^{5/3}}$$

where M_{BH} as the central BH mass, and \dot{M}_{fbt} as the templates of fallback material rates created for standard case with central BH of $M_{BH} = 10^6 M_\odot$ and disrupted main-sequence star of $M_* = 1 M_\odot$ and with a grid of the listed impact parameters β_{temp} in Guillochon & Ramirez-Ruiz (2013), and T_v as the viscous time after considering the viscous delay effects as discussed in

Guillochon & Ramirez-Ruiz (2013); Mockler et al. (2019). Here, a grid of 31 $\log(T_{v,temp}/\text{years})$ range from -3 to 0 are applied to create templates of \dot{M}_{at} for each impact parameter. Finally, templates of \dot{M}_{at} include 736 (640) time-dependent viscous-delayed accretion rates for 31 different T_v of each 23 (20) impact parameters for the main-sequence star with polytropic index γ of 4/3 (5/3).

Second, simple linear interpolations are applied to determine accretion rates $\dot{M}_a(T_v, \beta)$ for TDEs with input β and T_v different from the list values in β_{temp} and in $T_{v,temp}$. Assuming β_1, β_2 in the β_{temp} as the two values nearer to the input β and T_{v1}, T_{v2} in the $T_{v,temp}$ as the two values nearer to the input T_v , the first linear interpolation is applied to find the viscous-delayed accretion rates with input T_v but with $\beta = \beta_1$ and $\beta = \beta_2$ by

$$\begin{aligned}\dot{M}_a(T_v, \beta_1) &= \dot{M}_{at}(T_{v1}, \beta_1) + \\ &\frac{T_v - T_{v1}}{T_{v2} - T_{v1}} (\dot{M}_{at}(T_{v2}, \beta_1) - \dot{M}_{at}(T_{v1}, \beta_1)) \\ \dot{M}_a(T_v, \beta_2) &= \dot{M}_{at}(T_{v1}, \beta_2) + \\ &\frac{T_v - T_{v1}}{T_{v2} - T_{v1}} (\dot{M}_{at}(T_{v2}, \beta_2) - \dot{M}_{at}(T_{v1}, \beta_2))\end{aligned}\quad (2)$$

Then, the second linear interpolation is applied to find the viscous-delayed accretion rates with input T_v and with input β by

$$\dot{M}_a(T_v, \beta) = \dot{M}_a(T_v, \beta_1) + \frac{\beta - \beta_1}{\beta_2 - \beta_1} (\dot{M}_a(T_v, \beta_2) - \dot{M}_a(T_v, \beta_1)) \quad (3)$$

Third, for TDEs with input M_{BH} and M_* different from $10^6 M_\odot$ and $1 M_\odot$, as discussed in Guillochon & Ramirez-Ruiz (2013); Mockler et al. (2019), the actual viscous-delayed accretion rates \dot{M} and the corresponding time information are created from the viscous-delayed accretion rates $\dot{M}_a(T_v, \beta)$ by the following scaling ratios applied with input BH mass, mass and radius of the disrupted main-sequence star,

$$\begin{aligned}\dot{M} &= M_{BH,6}^{-0.5} \times M_*^2 \times R_*^{-1.5} \times \dot{M}_a(T_v, \beta) \\ t &= (1+z) \times M_{BH}^{0.5} \times M_*^{-1} \times R_*^{1.5} \times t_a(T_v, \beta)\end{aligned}\quad (4)$$

, where $M_{BH,6}$, M_* , R_* and z represent central BH mass in unit of $10^6 M_\odot$, stellar mass in unit of M_\odot , stellar radius in unit of R_\odot and redshift of host galaxy of a TDE, respectively. And the mass-radius relation discussed in Tout (1996) has been accepted in the manuscript for main-sequence stars.

Fourth, the time-dependent output emission spectrum in rest frame based on the TDE model expected accretion rate $\dot{M}(t)$ can be determined by the simple black-body photosphere model as discussed in Guillochon et al. (2014); Mockler et al. (2019),

$$\begin{aligned}F_\lambda(t) &= \frac{2\pi G c^2}{\lambda^5} \frac{1}{\exp(hc/(k\lambda T_p(t))) - 1} \left(\frac{R_p(t)}{D}\right)^2 \\ R_p(t) &= R_0 \times a_p \left(\frac{\epsilon \dot{M}(t) c^2}{1.3 \times 10^{38} M_{BH}/M_\odot}\right)^{l_p} \\ T_p(t) &= \left(\frac{\epsilon \dot{M}(t) c^2}{4\pi \sigma_{SB} R_p^2}\right)^{1/4} \quad a_p = (GM_{BH} \times (\frac{t_p}{\pi})^2)^{1/3}\end{aligned}\quad (5)$$

where D means the distance to the earth calculated by redshift z , k is the Boltzmann constant, $T_p(t)$ and $R_p(t)$ represent the time-dependent effective temperature and radius of the photosphere, respectively, and ϵ is the energy transfer efficiency smaller than 0.4, σ_{SB} is the Stefan-Boltzmann constant, and t_p is the time information of the peak accretion. Then, time-dependent apparent SDSS *ugriz*-band magnitudes $mag_u, g, r, i, z(t)$ can be well determined through the $F_\lambda(t)$ in observer frame convoluted with the accepted transmission curves of the SDSS *ugriz* filters.

Based on the four steps above, TDE model expected time dependent apparent *ugriz*-band magnitudes $mag_u, g, r, i, z(t)$ can be well created with seven parameters (redshift $z = 1.0624$ accepted to SDSS J0141) of central BH mass M_{BH} , mass M_* and polytropic index γ (4/3 or 3/5) of the disrupted main-sequence star, the impact parameter β , the viscous-delay time T_v , the energy transfer efficiency ϵ , and the two parameters of R_0 and l_p related to the black-body photosphere. Moreover, there are five additional parameters $mag_0(u, g, r, i, z)$, applied to determine contributions of host galaxies (the none-variability components included in the light curves) to observed variabilities.

Finally, through the Levenberg-Marquardt least-squares minimization technique (the MPFIT package) (Markwardt 2009), the theoretical TDE model can be well applied to describe the SDSS *ugriz*-band light curves. Meanwhile, when the fitting procedure above is applied, there is one limitation to the model parameters. For an available TDE, the determined tidal disruption radius is limited to be larger than event horizon of central BH. Then, the determined TDE model parameters (with $\gamma = 5/3$) and the corresponding uncertainties (1sigma errors computed from the covariance matrix) are: $\log(M_{BH,6}) \sim 1.16 \pm 0.05$, $\log(M_*/M_\odot) \sim -0.31 \pm 0.04$, $\log(\beta) \sim 0.39 \pm 0.01$, $\log(T_v) \sim -0.81 \pm 0.05$, $\log(\epsilon) \sim -0.55 \pm 0.05$, $\log(R_0) \sim -0.41 \pm 0.06$, $\log(l_p) \sim -0.14 \pm 0.06$, $\log(mag_0(u)) \sim 1.32 \pm 0.01$, $\log(mag_0(g)) \sim 1.32 \pm 0.01$, $\log(mag_0(r)) \sim 1.31 \pm 0.01$, $\log(mag_0(i)) \sim 1.31 \pm 0.01$, $\log(mag_0(z)) \sim 1.31 \pm 0.01$. Fig. 1 shows the TDE model determined best-fitting results and the corresponding confidence bands by uncertainties of the model parameters.

Before the end of the section, three points are noted. First, as discussed in Rumbaugh et al. (2018), SDSS J0141 has been classified as an extreme variability quasar (EVQ). Based on the improved DRW (Damped Random Walk) process in Kozłowski et al. (2010); Zu et al. (2013), the public JAVELIN (Just Another Vehicle for Estimating Lags In Nuclei) code can lead to best descriptions to the light curves of SDSS J0141. Here, in top middle panel of Fig. 1, the JAVELIN code determined best descriptions and corresponding confidence bands are shown as solid and dashed blue lines. Meanwhile, through the MCMC (Markov Chain Monte Carlo, Foreman-Mackey et al. (2013)) analysis with the uniform logarithmic priors of the DRW process parameters of τ and σ ($SF_\infty \sim \sigma\sqrt{\tau}$ as the parameter used in Rumbaugh et al. (2018)), bottom right panel of Fig. 1 shows the posterior distributions of σ and τ , with $\log(\tau/\text{days}) \sim 3.04$ and $\log(\sigma/(mag/\text{days}^{0.5})) \sim -0.535$, leading to the determined $\log(SF_\infty/mag) \sim 0.98$ which is about 1 magnitude larger than the shown results in Fig. 9 in Rumbaugh et al. (2018), indicating SDSS J0141 should have unique variabilities among the EVQs.

Second, an interesting method is applied to check whether the shown variabilities in Fig. 1 is not from TDE but actually from intrinsic AGN activities. Based on the CAR (continuous Autoregressive) process preferred to describe AGN variabilities discussed in Kelly et al. (2009):

$$dLMC_t = \frac{-1}{\tau} LMC_t dt + \sigma_* \sqrt{dt} \epsilon(t) + 19.77 \quad (6)$$

where $\epsilon(t)$ a white noise process with zero mean and variance equal to 1, and 19.77 is the mean value of LMC_t (the mean value of the SDSS *r*-band light curve of SDSS J0141)(different mean values in different bands have few effects on our following results). Then, a series of 1000 simulating light curves $[t_i, LMC_i]$ can be created, with randomly selected values of τ from 50days to 5000days (similar as the reported values of extreme variability quasars in Rumbaugh et al.

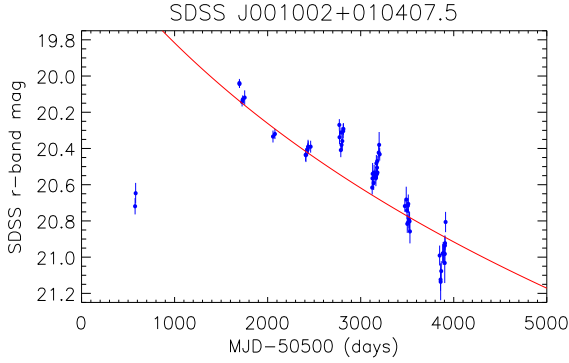


Figure 2. The r -band light curve of SDSS J001002+010407.5 as a TDE candidate collected from S82Qs. Solid red line shows the trend described by $t^{-5/3}$ as TDE model expected.

(2018)) and σ_* leading the variance $\tau\sigma_*^2/2$ to be 0.095 (the variance of SDSS r -band light curve of SDSS J0141), and t_i are the same as the observational time information shown in Figure 1. Among the 1000 simulating light curves, 4 light curves can be well described by theoretical TDE model, based on the criterion that the TDE-model determined best descriptions lead χ^2/DoF to be better than 3 (2.5 for the results shown in Fig. 1). Therefore, the probability is only about 0.4% (4/1000) that the detected TDE-expected variabilities in SDSS J0141 is mis-detected through the intrinsic AGN variabilities. Moreover, in order to confirm the probability of 0.4%, all the 9258 quasars covered in the Stripe82 region (S82Qs) (MacLeod et al. 2010) have their light curves been carefully checked. Among the 4763 S82Qs with light curves having number of available data points larger than 60, there are 11 quasars of which light curves have smooth declining trends $t^{-5/3}$ as TDE model expected. The number ratio of TDE candidates among the S82Qs is about 11/4763 \sim 0.23%, to support the expected ratio of 0.4% determined by the CAR simulating results. Fig. 2 shows the light curve of one of the 11 TDE candidates among the S82Qs. Detailed discussions on the TDE candidates among the S82Qs are beyond scope of the Letter and will appear in our manuscript in preparation. Therefore, the TDE expected variabilities in SDSS J0141 are confident enough.

Third, besides the SDSS long-term variabilities, within searching radius smaller than $1''$, long-term variabilities of SDSS J0141 have been collected from PanSTARRS with MJD from 55174 (Dec. 2009) to 56989 (Nov. 2014) shown as solid red circles in Fig. 1. The PanSTARRS data points can be well followed by the TDE model, besides the PanSTARRS g -band data points, perhaps due to large magnitude difference relative to quite different g -filter transmission curves between SDSS and PanSTARRS. Moreover, within searching radius smaller than $5''$, long-term variabilities can be collected from the PTF in Nov. 2014, from the WISE (Wide-field Infrared Survey Explorer) with MJD from 55207 (Jan. 2010) to 55570 (Jan. 2011), and from the ZTF (Zwicky Transient Facility) with MJD from 58307 (Sep. 2018) to 59543 (Nov. 2021), shown in Fig. 3 with none apparent variabilities. The long-term none-variabilities not only can be well expected by TDE model at late times, but also can be accepted as indirect evidence to support that the variabilities shown in Fig. 1 are not from intrinsic AGN variabilities. Furthermore, based on the WISE data points shown in the left panel of Fig. 3, the parameter $w1 - w2$ is about 1.22mag, a normal value applied to classify AGN by WISE colors (Assef et al. 2018). Meanwhile, as the reported MIR flares related to TDEs in Wang et al. (2018), WISE colors can be well around $w1 - w2 \sim 1\text{mag}$ (see their table 1). Therefore, only based

on the WISE colors, it is hard to provide further evidence to confirm that the variabilities in SDSS J0141 are not related to a central TDE but totally related to intrinsic AGN activities. However, based on the TDE model expected variabilities from SDSS and the more recent 7.4years-long none-variabilities from PTF and ZTF, the central TDE is preferred in SDSS J0141.

4 VIRIAL BH MASS FROM SPECTROSCOPIC PROPERTIES OF SDSS J0141

SDSS spectra of SDSS J0141 observed in MJD=52644, 53265, 53315, 57364, 58108 are shown in Fig. 4 with broad Mg II emission lines at $z = 1.0624$. Moreover, for the spectrum with MJD=58108, continuum emissions can be described by $2.66 \times \lambda^{-0.19}$, leading continuum luminosity at rest wavelength 3100\AA to be about $\lambda L_{3100} \sim 5.01 \times 10^{44}\text{erg/s}$.

Through broad Mg II emission lines, virial BH mass as discussed in Peterson et al. (2004); Shen et al. (2011) can be estimated as

$$\log\left(\frac{M_{BH}}{M_\odot}\right) = 0.86 + 0.5 \log\left(\frac{\lambda L_{3100}}{10^{44}\text{erg/s}}\right) + 2 \log\left(\frac{FWHM}{\text{km/s}}\right) \quad (7)$$

$$\sim 8.39$$

with $FWHM \sim 3900\text{km/s}$ measured through the definition of Full Width at Half Maximum (FWHM) for the broad Mg II from the spectrum observed in MJD=58108 after subtraction of the power law continuum emissions. Based on the results in Fig. 1, the spectrum with MJD=58108 has few effects of the central TDE. The estimated virial BH mass is about 18 times larger than the TDE-model determined BH mass, indicating apparent contributions of TDE fallback accreting debris to broad Mg II emission clouds. The distance of the broad Mg II emission clouds to central BH could be quite smaller than the Virialization assumption expected BLRs sizes, leading to quite larger Virial BH mass in SDSS J0141, similar as what have been discussed in SDSS J0159 in Zhang et al. (2019); Zhang (2021).

Actually, it is still an open question whether the TDE model determined BH masses are well consistent with intrinsic BH masses in TDE candidates. However, Guillochon et al. (2014); Mockler et al. (2019); Ryu et al. (2020); Zhou et al. (2021) have shown that the long-term TDE model expected variabilities can be well applied to estimate central BH masses of TDE candidates. Meanwhile, for SDSS J0141 at redshift 1.06, there is no way to measure stellar velocity dispersion in SDSS spectra, indicating that it is hard to measure more reliable BH mass through the M-sigma relation (Ferrarese & Merritt 2000; Gebhardt et al. 2000; Kormendy & Ho 2015) in SDSS J0141. Therefore, in the Letter, TDE model determined BH mass and Virial BH mass are compared in SDSS J0141. Certainly, further efforts are necessary to determine accurate central BH mass which will provide further clues to support or to against the central expected TDE in the SDSS J0141.

5 CONCLUSIONS

Finally, we give our main conclusions as follows. A preferred TDE can be well applied to describe the long-term SDSS $ugriz$ -band variabilities over 8 years in the SDSS J0141 with apparent broad Mg II emission lines at $z = 1.06$, leading the TDE model determined BH mass to be about $(14 \pm 2) \times 10^6 M_\odot$. Moreover, based on CAR process created artificial light curves, the probability is only about 0.4% that the long-term variabilities in SDSS J0141 are from central AGN activities but not from a central TDE. Meanwhile, through the

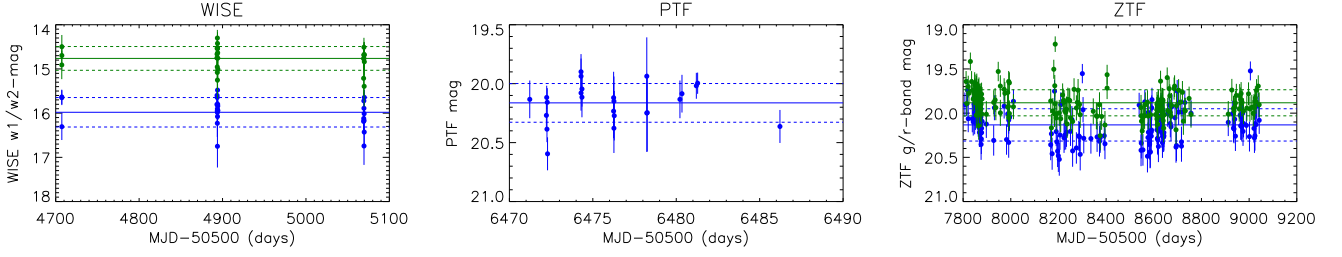


Figure 3. The collected data points from WISE (w1 in blue, w2 in dark green), PTF and ZTF (g-band in blue, r-band in dark green). In each panel, horizontal solid line and dashed lines show the mean value and the range of standard deviation.

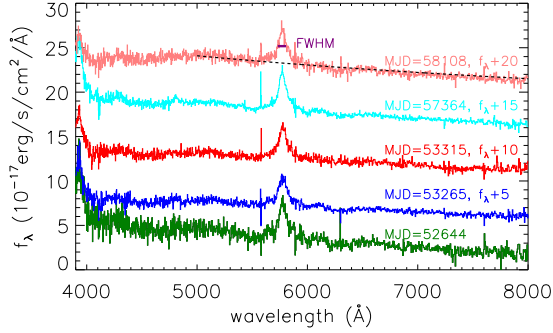


Figure 4. The SDSS spectra in five different epochs. Dashed black line shows the power law described continuum emissions in the SDSS spectrum with MJD=58108. Horizontal purple line marks the width of FWHM of broad Mg II in the SDSS spectrum with MJD=58108.

broad Mg II emission lines, the virial BH mass can be estimated to be about $245 \times 10^6 M_{\odot}$, about 18times larger than the TDE-model determined BH mass, providing further clues to support the central TDE in SDSS J0141. Among the reported optical TDE candidates, SDSS J0141 is the candidate with the highest redshift. Moreover, it is feasible to detect more TDE candidates in galaxies with broad emission lines, not only broad Balmer lines and Helium lines but also broad Mg II lines.

ACKNOWLEDGEMENTS

Zhang gratefully acknowledges the anonymous referee for giving us constructive comments and suggestions to greatly improve our paper. Zhang gratefully acknowledges the grant support from NSFC-12173020. This Letter has made use of the data from the SDSS projects managed by the Astrophysical Research Consortium for the Participating Institutions of the SDSS-III Collaboration. The letter has made use of the public code of TDEFIT and MOSFIT, and MPFIT. This Letter has made use of the data from PanSRARRS, WISE, PTF and ZTF.

DATA AVAILABILITY

The data underlying this article will be shared on reasonable request to the corresponding author (aexueguang@qq.com).

REFERENCES

- Anderson, M., Mooley, K., Hallinan, G., et al., 2020, *ApJ*, 903, 116 – 127
 Assef, R. J.; Stern, D.; Noiro, G.; Jun, H.; Cutri, R.; Eisenhardt, P., 2018, *ApJS*, 234, 23
 Blagorodnova, N.; Gezari, S.; Hung, T.; et al., 2017, *ApJ*, 844, 46
 Bramich, D. M.; Vidihi, S.; Wyrzykowski, L., et al., 2008, *MNRAS*, 386, 887
 Chornock, R.; Berger, E.; Gezari, S.; et al., 2014, *ApJ*, 780, 44
 Ferrarese, F. & Merritt, D., 2000, *ApJL*, 539, 9
 Gebhardt, K., et al., 2000, *ApJL*, 539, 13
 Foreman-Mackey, D.; Hogg, D. W.; Lang, D.; Goodman, J., 2013, *PASP*, 125, 306
 Gezari, S.; Martin, D. C.; Milliand, B., et al., 2006, *ApJL*, 653, 25
 Gezari, S.; Chornock, R.; Rest, A., et al., 2012, *Nature*, 485, 217
 Gezari, S., 2021, *ARA&A*, 59, 21
 Gromadzki, M.; Hamałowicz, A.; Wyrzykowski, L.; et al., 2019, *A&A*, 622, 2
 Guillochon, J.; & Ramirez-Ruiz, E., 2013, *ApJ*, 767, 25
 Guillochon, J.; Manukian, H.; Ramirez-Ruiz, E., 2014, *ApJ*, 783, 23
 Hinkle, J. T., et al., 2021, *MNRAS*, 500, 1673
 Holoien, T. W., et al., 2014, *MNRAS*, 445, 3263
 Holoien, T. W. S.; Kochanek, C. S.; Prieto, J. L.; et al., 2016, *MNRAS*, 455, 2918
 Holoien, T. W. S.; Huber, M. E.; Shappee, B. J.; et al., 2019, *ApJ*, 880, 120
 Hung, T.; Foley, R. J.; Ramirez-Ruiz, E.; et al., 2020, *ApJ*, 903, 31
 Kelly, B. C.; Bechtold, J.; Siemiginowska, A., 2009, *ApJ*, 698, 895
 Kormendy, J. & Ho, L. C., 2013, *ARA&A*, 51, 511
 Kozłowski, S., et al., 2010, *ApJ*, 708, 927
 Liu, F. K.; Zhou, Z. Q.; Cao, R.; Ho, L. C.; Komossa, S., 2017, *MNRAS Letter*, 472, 99
 Loeb, A.; Ulmer, A., 1997, *ApJ*, 489, 573
 MacLeod, C. L.; Ivezić, Z.; Kochanek, C. S., et al., 2010, *ApJ*, 721, 1014
 Markwardt, C. B., 2009, *ASPC*, 411, 251
 Merloni, A.; Dwelly, T.; Salvato, A. G.; et al., 2015, *MNRAS*, 452, 69
 Mockler, B.; Guillochon, J.; Ramirez-Ruiz, E., 2019, *ApJ*, 872, 151
 Peterson, B. M., et al., 2004, *ApJ*, 613, 682
 Rumbaugh, N.; Shen, Yue; Morganson, E.; et al., 2018, *ApJ*, 854, 160
 Rees, M. J., 1988, *Nature*, 333, 523
 Ryu, T.; Krolik, J.; Piran, T., 2020, *ApJ*, 904, 73
 Sazonov, S.; Gilfanov, M.; Medvedev, P.; et al., 2021, *MNRAS*, 508, 3820
 Shen, Y.; Richards, G. T.; Strauss, M. A.; et al., 2011, *ApJS*, 194, 45
 Short, P.; Nicholl, M.; Lawrence, A.; Gomez, S.; et al., 2020, *MNRAS*, 498, 4119
 Stone, N. C.; Kesden, M.; Chang, R. M.; van Velzen, S.; General Relativity and Gravitation, 2019, 51, 30, arXiv:1801.10180
 Tout, C. A.; Pols, O.; Eggleton, P.; Han, Z., 1996, *MNRAS*, 281, 257
 van Velzen, S.; Farrar, Glennys R.; Gezari, S., et al., 2011, *ApJ*, 741, 73
 van Velzen, S.; Gezari, S.; Hammerstein, E.; et al., 2021, *ApJ*, 908, 4
 Wang, T.; Yan, L.; Dou, L., et al., 2018, *MNRAS*, 477, 2943
 Zhang, X. G.; Bao, M.; Yuan, Q. R., 2019, *MNRAS Letter*, 490, 81
 Zhang, X. G.; 2021, *MNRAS Letter*, 500, 57
 Zhang, X. G.; 2021b, *ApJ*, 919, 13, arXiv: 2107.09214

Zhang, X. G.; 2022, ApJ accepted, Arxiv:2202.11265

Zhou, Z. Q.; Liu, F. K.; Komossa, S., et al., 2021, ApJ, 907, 77

Zu, Y.; Kochanek, C. S.; Kozłowski, S.; Udalski, A., 2013, ApJ, 765, 106